Volume 27
Number 32
28 August 2025
Pages 16695–17084

PCCP

Physical Chemistry Chemical Physics

rsc.li/pccp

25 YEARS ANNIVERSARY

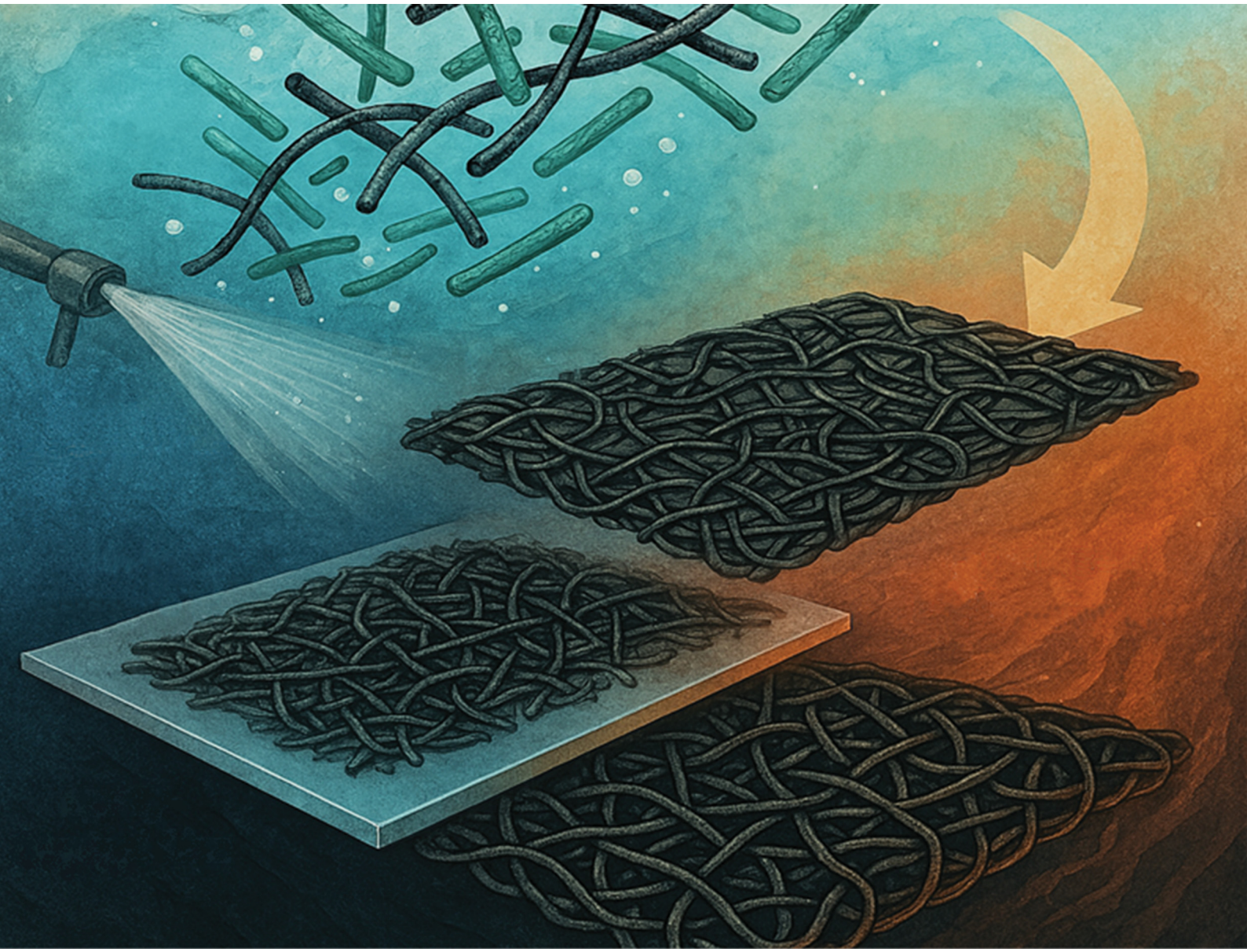

ISSN 1463-9076

ROYAL SOCIETY OF CHEMISTRY

PAPER

Alejandro Ansón-Casaos,
José Miguel González-Domínguez *et al.*
Carbon nanotube film electrodes enabled by nanostructured biopolymers through aqueous processing

PCCP Owner Societies

PCCP

ROYAL SOCIETY OF CHEMISTRY

PAPER

View Article Online
View Journal | View Issue

Cite this: *Phys. Chem. Chem. Phys.*, 2025, **27**, 16756

Carbon nanotube film electrodes enabled by nanostructured biopolymers through aqueous processing†

Carlos Martínez-Barón, [a] Víctor Calvo, [a] Miguel Ángel Álvarez-Sánchez, [a] F. Javier Pascual, [b] Wolfgang K. Maser, [a] Ana M. Benito, [a] Alejandro Ansón-Casaos *[a] and José Miguel González-Domínguez *[a]

Received 22nd April 2025,
Accepted 2nd July 2025

DOI: 10.1039/d5cp01536g

rsc.li/pccp

Processing carbon nanotubes (CNTs) into conductive films *via* liquid-phase is highly attractive for the fabrication of electronic and electrochemical device components. However, conventional deposition methods usually suffer from several limitations, including environmental concerns, loss of intrinsic properties, and poor reproducibility. Nanostructured biopolymers (NBs), such as cellulose (CNCs) and chitin (ChNCs) nanocrystals, offer an environmentally friendly strategy for dispersing CNTs in water alternative to organic solvents, surfactants or chemical functionalization. In this work, we present the first direct comparison of conductive and electroactive films resulting from using CNCs and ChNCs as dispersing agents for both single-walled and multi-walled CNTs. The as-made aqueous dispersions are used as inks to fabricate CNT/NB films *via* spray coating, achieving excellent homogeneity, controllable film thickness, and sheet resistances mostly below 130 $\Omega\ \square^{-1}$. Furthermore, we demonstrate that post-deposition thermal treatment at 450 °C in an inert atmosphere effectively pyrolyzes the non-conductive NB matrix while increasing contacts between CNTs in the network, leading to enhanced electrical conductivities and electrochemically active surface areas. These findings highlight NBs as greener processing agents for the formulation of waterborne CNT inks and emphasize their relevance for the controlled and sustainable fabrication of conductive films and electrodes.

Introduction

Carbon nanotubes (CNTs) have shown remarkable potential across electronic, optoelectronic, and catalytic applications, and have been widely investigated in sensors, transistors and energy management.[1–6] Their exceptional versatility arises from their sp^2-hybridized carbon framework, which endows them with high aspect ratio, outstanding mechanical and thermal stability, and excellent electrical conductivity.[7,8] These properties enable CNTs to be processed into functional films, providing a scalable route to transfer their intrinsic nanoscale functionalities into device architectures, typically *via* liquid-phase processing.[9–12] However, conventional fabrication methods often rely on toxic or non-renewable solvents, surfactants, or additives and face issues related to reproducibility, durability, and scalability, limiting their broader application.[13–15]

CNT films, in particular, have proven highly suitable as conductive electrodes due to their efficient charge transport, structural integrity, and robustness under mechanical and chemical stress.[4,16,17] Beyond their conductive role, CNTs have also been explored as catalyst supports and even as metal-free catalysts, owing to their high surface area and the potential for heteroatom doping.[5,18] This dual functionality is especially valuable in electrochemical processes, where CNT films can serve simultaneously as the catalytic interface and the current collector, providing both high conductivity and significant electrochemical activity.

Given these limitations, there is a clear need to develop sustainable and scalable strategies for the fabrication of single-walled CNT (SWCNT) and multi-walled CNT (MWCNT) films that are both cost-effective and reproducible. A promising approach to overcome the limitations of conventional processing involves the use of nanostructured biopolymers (NBs) to stabilize CNTs in water, avoiding chemical functionalization, organic solvents or surfactants.[19] NBs are a class of naturally derived macromolecules that possess nanoscale dimensions and well-defined morphologies, which increase their properties compared to their microscale counterparts.[20–23] Representative

[a] *Instituto de Carboquímica (ICB-CSIC), Miguel Luesma Castán 4, 50018, Zaragoza, Spain. E-mail: alanson@icb.csic.es, jmgonzalez@icb.csic.es*
[b] *Centro Universitario de la Defensa de Zaragoza, Academia General Militar, Zaragoza, 50090, Spain*

† Electronic supplementary information (ESI) available. See DOI: https://doi.org/10.1039/d5cp01536g

examples include cellulose nanocrystals (CNCs),[22,24] chitin nanocrystals (ChNCs),[21] and nanoscale derivatives of other polysaccharides,[23,25] silk fibroin,[26–29] and DNA.[30,31]

Previous studies have demonstrated the effectiveness of CNCs prepared *via* sulfuric acid hydrolysis as efficient dispersing agents for CNTs and related carbon nanomaterials.[19,32–36] This acidic hydrolysis method provides a green and straightforward synthesis approach and enables the preparation of different CNC allomorphs (mainly crystalline types I and II) by adjusting the reaction conditions.[34,37] To date, most works have focused exclusively on the use of type I CNCs for dispersing CNTs, while our group has recently proposed the use of type II CNCs for this purpose, yielding highly stable aqueous colloids.[19,34,35,38] These CNT/CNC dispersions have shown potential for various applications, including electrochemical sensors,[38] conductive thin films[33,39] and biomedicine.[40] In contrast, the use of ChNCs for dispersing CNTs has remained largely unexplored, with only two studies reported to date.[41,42] The first study focused on MWCNTs and demonstrated the fabrication of a paper-based thermoelectric generator by screen-printing,[41] while the second, conducted by our group, extended the use of ChNCs to other carbon nanomaterials, such as SWCNTs and carbon nanofibers, and evaluated their suitability for electrode fabrication *via* spray-coating.[42] Other NBs, such as CNCs and cellulose nanofibers prepared *via* TEMPO-mediated oxidation,[43–48] as well as silk fibroin nanofibers,[49,50] have also shown promise for CNT dispersion, further supporting the potential of NBs as versatile and sustainable processing agents of CNTs in water.

This work presents the first direct comparison between ChNCs and both main allomorphs of CNCs as dispersing agents for SWCNTs and MWCNTs, respectively, in aqueous media, analyzing the morphology, surface chemistry, and stability of the resulting dispersions. These dispersions are subsequently used as inks to fabricate conductive films *via* spray-coating, and the effect of post-deposition thermal treatment under an inert atmosphere is investigated as a means to further enhance the electrical conductivity and electrochemically active surface area of the films. Our findings underscore the potential of this green strategy for developing CNT films and electrodes with tailored electrical and electrochemical properties using exclusively aqueous media and green nanomaterial adjuvants.

Experimental

Materials and reagents

Microcrystalline cellulose (MCC, ref. 310697) with an average particle size of 20 μm and chitin extracted from shrimp shells (Practical grade, powder; C7170) were purchased from Sigma-Aldrich. H_2SO_4 98 wt% (SUAC-00A), HCl 37% (CHAC-0AI) and NaOH pearls (SOHY-P0T) were purchased from Labkem (Spain). Ultrapure water, purified using a Siemens Ultraclear device, was used for all the experimental procedures. Dialysis membranes were purchased from Merck (average flat width 33 mm, D9652-100FT). SWCNTs were acquired from Carbon Solutions Inc. (Purified, ref. P2-SWNT). According to the manufacturer, P2-SWNTs are first obtained through the arc discharge method using graphite as the starting material and then purified by a non-disclosed method resulting in a very low oxidation degree with carbon purity of over 90% and a significantly decreased metal content ranging from 4% to 8%. MWCNTs were purchased from Nanocyl (NC 7000™).

Synthesis of type I and II CNCs

Type I (cellulose chains oriented in parallel within the crystalline domain) and type II (antiparallel chain arrangement) CNCs were prepared *via* acidic hydrolysis with H_2SO_4 following a previously described protocol.[37] In a typical experiment, 10 g of MCC were dispersed in 45 mL of water, and H_2SO_4 was added at 0 °C. Type I CNCs were obtained by rapidly adding 45 mL of H_2SO_4 (under 5 minutes), followed by a 10-minute reaction at 70 °C, whereas type II CNCs were produced by slowly adding the same amount of H_2SO_4 and reacting for 1 hour at ambient temperature. After hydrolysis, the mixture was poured into 1 L of ultrapure water and left to decant overnight at 4 °C. The decanted bottom liquid was then dialyzed against ultrapure water until a neutral pH was reached, followed by several centrifugation cycles at 9000 rpm (9327 rcf) for 1 minute each. Finally, the dispersions were freeze-dried to estimate the concentration and to obtain CNCs in powder form.

Synthesis of ChNCs

ChNCs were prepared by acidic hydrolysis using HCl, following a recently described protocol.[42] In a typical procedure, 4 g of chitin powder were added to 80 mL of 3 M HCl and refluxed at 120 °C for 90 minutes. After hydrolysis, the mixture was poured into 1 L of ultrapure water and left to decant overnight at 4 °C. The suspension was then dialyzed against ultrapure water until neutral pH was reached, followed by centrifugation at 9000 rpm (9327 rcf) for 20 minutes. The resulting solids were redispersed in ultrapure water and subjected to two centrifugation and redispersion cycles. Finally, the dispersion was freeze-dried to determine the concentration and yield and to obtain the ChNCs in powder form for further use.

Surface conditioning of MWCNTs

To improve the hydrophilicity of MWCNTs, and improve their compatibility with NBs as well, a surface conditioning process was conducted prior to their use as described in a prior publication.[42] Briefly, MWCNTs were subjected to a mild oxidation treatment using diluted HNO_3 under reflux, a widely used method for CNT purification.[51,52] In this process, MWCNTs were added to a 1.5 M HNO_3 solution and refluxed for 90 minutes. The mixture was then filtered through Isopore™ Membrane Filters (10 μm TCTP), rinsed with ultrapure water, and dried overnight at 65 °C. From this point forward, "p-MWCNTs" will denote the treated MWCNTs.

Preparation of CNT/NB dispersions

The optimization of CNT/ChNC dispersions was previously reported in a recent publication,[42] while the optimization of

P2-SWCNT/CNC (Fig. S1) and p-MWCNT/CNC (Fig. S2) is detailed in the ESI.† According to a standard protocol, dispersions were prepared by mixing different concentrations of NBs (1–5 g L^{-1}) in solid form with 1 g L^{-1} of each kind of CNT. Ultrapure water was then added, and the dispersion process was assisted by a sonication step using an ultrasound tip (Hielscher DRH-P400S) at 60% amplitude and 0.5 cycle. To minimize heating, the dispersion was maintained in an ice/water bath, with intermittent manual shaking and bath sonication. To separate non-stabilized particles and eventually obtain stable dispersions, the suspensions were centrifuged at 4000 rpm (1842 rcf) for 4 minutes. For both type I CNC- and type II CNC-based dispersions, an additional redispersion step was required to achieve a successful dispersion. This step consists of centrifugation at 12 000 rpm for 30 minutes to fully sediment the solid material. The supernatant was decanted off, and the pellet was dispersed again in fresh ultrapure water, followed by bath ultrasounds to ensure complete redispersion. Afterward, the CNT/CNC dispersions were centrifuged again at 4000 rpm (1842 rcf) for 4 minutes.

Characterization of CNT/NB dispersions

Diluted CNT/NB dispersions were characterized immediately after preparation using UV-vis spectroscopy, dynamic light scattering (DLS), and ζ-potential measurements. UV-Vis spectroscopy was conducted on a Shimadzu UV-2401PC spectrophotometer to estimate the concentration of CNTs based on their absorbance ratios at 850 nm compared to the non-centrifuged dispersions. DLS and ζ-potential measurements were performed using a Malvern Nano ZS instrument, applying the refractive index of carbon (2.42). Each measurement was repeated at least three times to ensure accuracy, with an average pH of 4.6 and an ambient temperature of 25 °C maintained throughout the entire duration of the experiments. Transmission electron microscopy (TEM) images of the CNT/NB dispersions were acquired using a Tecnai T20 (Thermo Fisher) equipped with a 200 kV field emission electron gun. One or two droplets of the dispersions, previously diluted to 0.1 g L^{-1} CNTs, were placed onto a carbon-coated copper grid (LC200-CU Lacey/carbon 200 mesh, electron microscopy sciences), and left to dry in air at room temperature. The CNT/NB materials were freeze-dried, and the resulting solid was analyzed by X-ray diffraction (XRD), Raman spectroscopy, and thermogravimetric analysis (TGA). Moreover, the resulting solids were thermally treated at 450 °C for 30 min under a N_2 atmosphere for further characterization.

Structural and morphological characterization

XRD was conducted using a Bruker D8 Advance diffractometer in Bragg–Brentano geometry over the range of 2θ = (5°–50°), with steps of 0.05° and 3 s accumulation time. Raman spectroscopy was performed using a dispersive micro-Raman LabRam HR800 UV (Horiba Jobin Yvon), equipped with a 532 nm excitation laser operating at an output power of 0.7 mW, calibrated with a silicon standard. The setup included a CCD detector and a confocal microscope with a 100× objective lens and the sample was positioned on a diffraction grid of 600 g mm^{-1}. TGA was performed using a Netzsch TG 209F1 device, under a N_2 flow, with a heating rate of 10 °C min^{-1} from room temperature to 800 °C.

Preparation of CNT/NB films

Before casting the CNT/NB dispersions, hereafter referred to as inks, the glass substrates (1 cm × 2.5 cm) were cleaned by sequential immersion in acetone and isopropanol for 15 min each in an ultrasonic bath, and were then immediately dried with a N_2 stream. Then, the glass substrates were ozonized (Ossila UV Ozone Cleaner) for 15 min. Inks were deposited using a semi-automatic spray coater (Nadetech ND-SP Ultrasonic PRO) at a flow rate of 42 mL h^{-1}. The nozzle was placed 60 mm above the sample, and the temperature of the hotplate was set at 80 °C. Under these conditions, we were able to control the film thickness by adjusting the number of spray coating steps. Additionally, the resulting electrodes were thermally treated in a horizontal quartz reactor at 450 °C for 30 min under a N_2 flow.

Electrical characterization of the CNT/NB films

The sheet resistance (R_S) of the conductive films over glass was measured with an in-line 4-point probe configuration using a Keithley 4200 system with an equidistant probe separation of 2.24 mm. The surface morphology of films was evaluated using scanning electron microscopy (SEM) images, which were acquired directly, with no preparation procedure, before and after the thermal treatment with an INSPECT F50 at a voltage of 10 kV and a working distance of 8 mm without metallization. An evaluation of the film thickness was conducted by acquiring SEM images of the films at 90°.

Mechanical characterization of the CNT/NB films

Nanohardness (H) and elastic moduli (E) of the conductive films over glass were measured with a single indentation method using a Berkovich diamond tip in an Agilent G200 Nanoindenter with a matrix of 5 × 2 indentations, with an equidistant separation of 20 μm. The load was applied at a constant rate of 0.075 mN s^{-1} up to a maximum of 750 μN. A mean Poisson's ratio of 0.18 was assumed. The maximum indentation depth was recorded.

Electrochemical characterization of CNT/NB electrodes

Electrochemical measurements were carried out on a three-electrode cell configuration by using an Autolab PGSTAT 302N potentiostat (Metrohm AG, Herisau, Switzerland). The reference electrode was Ag/AgCl, 3 M NaCl (E^0 = 0.210 V), and the counter electrode was a platinum foil (geometric surface area: 0.8 cm^2). The CNT/NB film was connected to the potentiostat probe through a copper wire and a contact made of silver conductive inks. A 1 M solution of NaOH was used as the electrolyte, being previously purged with N_2 for 15 min prior to measurements. Cyclic voltammetry measurements were performed from 0.4 V to −0.1 V and the submerged electrode surface inside the electrolytic solution was approximately 0.5 cm^2.

The recorded current was divided by the geometrical surface area of the employed electrodes for data normalization. Electrochemical impedance spectroscopy measurements were carried out from 10^5 to 10^{-2} Hz using 0.1 M NaOH as the electrolyte, at a fixed potential of 0.2 V (*vs.* Ag/AgCl).

Results and discussion

The optimization of the CNT/NB dispersions involved several key steps designed to achieve fine and highly stable inks, with the aim of maximizing the CNT content, while minimizing the excess NBs, making it suitable for the fabrication of conductive films by spray coating. Different concentrations of NBs were tested to determine the optimal amount needed to effectively stabilize the CNTs in water. The concentrations of NBs used ranged from 1 to 5 g L^{-1}, while the concentration of CNTs was kept constant at 1 g L^{-1} in all experiments. In the case of MWCNTs, to improve their compatibility with NBs, they were mildly oxidized using diluted HNO_3 under reflux before being dispersed. This process, as described in previous publications,[42,51,52] enhances the hydrophilicity of CNTs, favoring their mixing in water with NBs. Then, the colloidal properties of the optimized CNT/NB dispersions were analyzed to understand the effectiveness of different NBs in stabilizing CNTs in aqueous media (Table 1). This study revealed important differences regarding the CNT concentrations in suspension, hydrodynamic radii and ζ-potential (Fig. S1 and S2, ESI†) depending on the type of NB used and the type of CNT being dispersed. These variations highlight the subtle interactions between CNTs and NBs, which are crucial for developing stable and functional inks. Specifically, type II CNCs consistently outperformed other NBs in stabilizing both p-MWCNTs and P2-SWCNTs, achieving higher CNT concentrations and providing stronger electrostatic stabilization. Among the full set of the prepared dispersions, the combination of P2-SWCNTs and type II CNCs resulted in the highest CNT concentration achieved (0.83 g L^{-1}), indicating a highly effective dispersion. The smaller hydrodynamic radii observed for P2-SWCNT/CNC II dispersions, compared to P2-SWCNT/CNC I, reflect a much more homogeneous dispersion, demonstrating that the type II allomorph of cellulose is particularly effective in stabilizing CNTs in water. ChNCs also exhibited slightly superior performance compared to type I CNCs, yielding lower hydrodynamic sizes, although lower ζ-potential in absolute values, indicating that steric interactions may play a somewhat greater role in their stabilization mechanism. The CNT/NB dispersions remained colloidally stable for over one year of storage at room temperature, as shown by DLS and ζ-potential measurements (Table S1, ESI†).

To further elucidate the nature of these interactions, TEM was employed to examine the morphological and structural characteristics of the CNT/NB hybrids (Fig. 1). The TEM images revealed distinct structural arrangements depending on the specific combination of CNTs and NBs. For example, p-MWCNT/ChNC hybrids formed a network of ChNCs surrounding the p-MWCNTs (Fig. 1A), while in P2-SWCNT/ChNC hybrids, the ChNCs appeared to discretely adsorb onto the SWCNTs, covering most of their surface and leading to their individualization and wrapping (Fig. 1B).[42] The interactions between type I CNCs and p-MWCNTs resulted in an expanded structure that immobilized the p-MWCNTs (Fig. 1C). In contrast, P2-SWCNT/CNC I hybrids showed more isolated CNTs with individual type I CNCs contacting their walls in a parallel arrangement (Fig. 1D).[34] Interestingly, the interaction between type II CNCs and p-MWCNTs seems to be more specific, and these CNCs are found only in the surroundings of p-MWCNTs (Fig. 1E), while type II CNCs also form an entangled network with P2-SWCNTs (Fig. 1F).[34] These diverse morphological characteristics underscore the importance of specific NB-CNT combinations in determining the overall structure of the resulting nanohybrids.

Following the colloidal and morphological characterization, the structural properties of the CNT/NB solid hybrids, obtained by lyophilization of the CNT/NB dispersions, were investigated using Raman spectroscopy, XRD, and TGA. Similar to the prepared films, these solid materials were thermally treated at 450 °C for 30 minutes to assess the impact of the thermal treatment on the structural features of the CNT/NB hybrid nanomaterials. In the case of Raman spectroscopy (Fig. S3, ESI†), the obtained spectra were coincident with those of their respective kind of nanotube, with no visible features of the employed NB. This is further discussed in the ESI.† Moreover, the D-band/G-band peak intensity ratio is also displayed (Table S2, ESI†), showing a generalized decrease after the thermal treatment, being an indicative of a reduction of the number of structural defects. Additional information of the structural integrity of the CNTs when stabilized within the dispersions can be acquired *via* UV-vis-NIR spectroscopy (Fig. S4, ESI†).

Table 1 Characterization results (CNT concentrations after centrifugation, hydrodynamic radii and ζ-potential) of the optimal composition for CNTs and NBs. Note that the initial concentration of CNTs is set to 1 g L^{-1} in all experiments

Type of CNT	NB	NBs initial conc. (g L^{-1})	CNT conc. after centrifugation (g L^{-1})	Hydrodynamic radii (nm)	ζ-Potential (mV)
p-MWCNTs	ChNCs	3.5	0.58 ± 0.03	130 ± 15	24 ± 2
	CNCs I	4	0.5 ± 0.1	179 ± 65	−23 ± 6
	CNCs II	3	0.8 ± 0.2	131 ± 29	−27 ± 8
P2-SWCNTs	ChNCs	3	0.54 ± 0.04	86 ± 3	23 ± 6
	CNCs I	3	0.32 ± 0.06	125 ± 22	−30 ± 3
	CNCs II	2	0.83 ± 0.07	108 ± 42	−33 ± 4

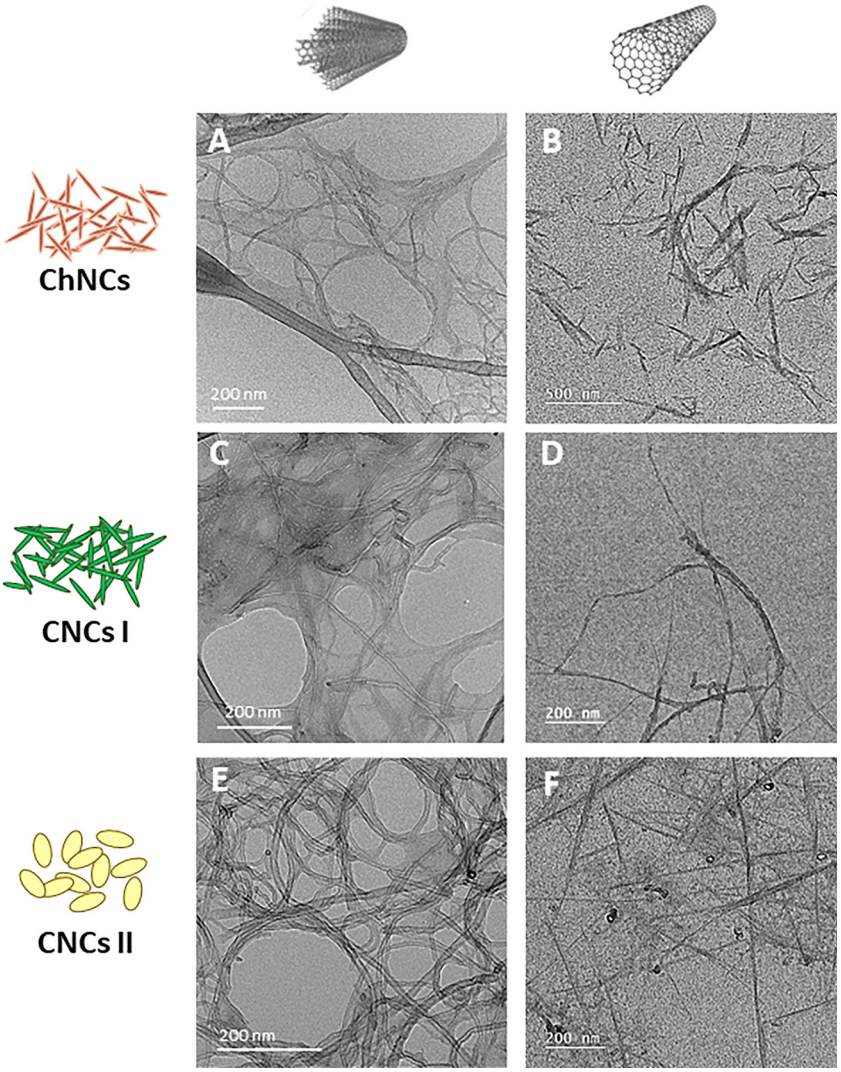

Fig. 1 TEM images of CNT/NB hybrids: (A) p-MWCNT/ChNC, (B) P2-SWCNT/ChNC, (C) p-MWCNT/CNC I, (D) P2-SWCNT/CNC I, (E) p-MWCNT/CNC II, and (F) P2-SWCNT/CNC II.

Only the SWCNTs present measurable features in this region, corresponding to their metallic (M) and semiconducting (S) van Hove transitions.[53] By inducing the separation of SWCNTs from the rest of carbon species through different centrifugation speeds, it is observed that the amount of stable SWCNTs in water can be very high owing to the effect of NBs, reaching optical purity ratios of almost two-fold at moderate speeds (Table S3, ESI†).

XRD analyses for the as-produced and thermally treated hybrids are shown in Fig. 2. XRD patterns of CNT/CNC I and CNT/ChNC hybrids exhibit diffractograms resembling those of their respective CNTs and NBs (Fig. S5, ESI†), with the slight emergence of a peak at $2\theta = 26^\circ$, corresponding to the graphitic (002) plane, characteristic of the interlayer stacking plane of graphite sheets, typical for MWCNTs, and ascribed to remaining graphite precursor impurities in SWCNTs. By contrast, the hybrids of CNTs with type II CNCs displayed a much more pronounced graphitic (002) peak, due to the higher CNT/NB ratio, alongside noticeable variations in the diffraction patterns of type II CNCs. After thermal treatment, the characteristic diffraction peaks of NBs disappeared entirely while enhancing the graphitic plane intensity, thus confirming the complete pyrolysis of the biopolymers. A worth noting aspect upon pyrolysis is the appearance of a prominent peak at around $2\theta = 4$–6° in the case of SWCNTs (Fig. 2B). This is a distinctive feature generated by the close packing of SWCNTs into crystalline bundles forming a triangular lattice,[54] and the absence of it before thermal treatment evidences a full de-aggregation of SWCNT ropes by the dispersive action of NBs in aqueous media, leading to exfoliation and eventual individualization of CNTs, which remains after the film deposition step. After thermally treating the films, it can be observed that regardless of the NB employed, this peak reappears (albeit somewhat weaker in the case of ChNCs), pointing to the re-assembly of the SWCNTs into large crystalline bundles, with the associated graphitic feature at $2\theta = 26^\circ$. This dispersion strategy allows

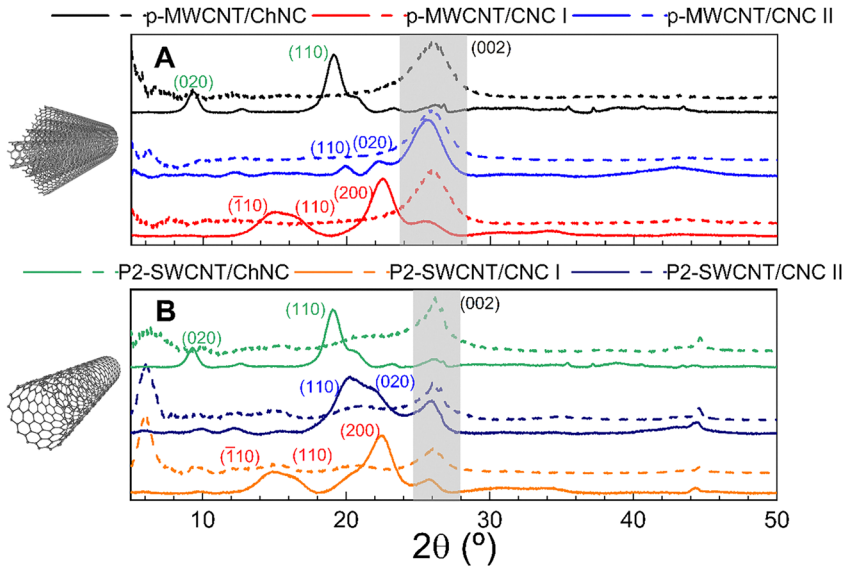

Fig. 2 XRD results of the freeze-dried (A) p-MWCNT/NB and (B) P2-SWCNT/NB dispersions before (solid line) and after the thermal treatment (dashed line). The region corresponding to the graphitic (002) plane has been shaded in gray, and the main diffraction planes of each NB are labeled as follows: ChNCs in green, type II CNCs in blue, and type I CNCs in red.

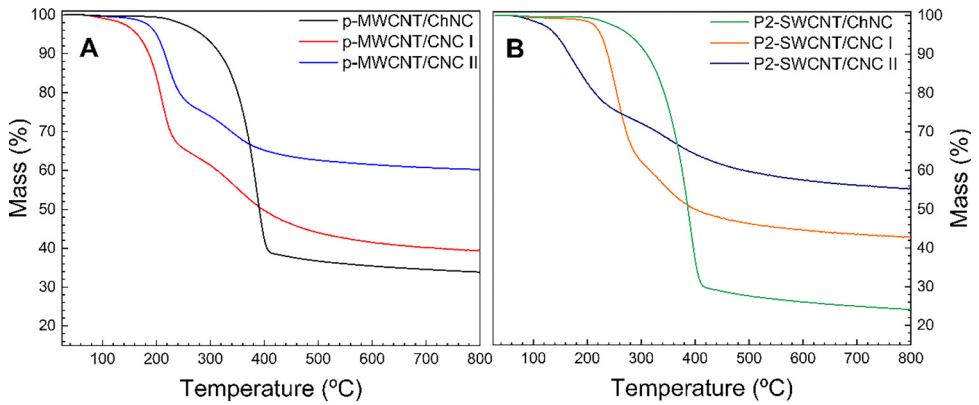

Fig. 3 TGA results under a N_2 atmosphere from ambient temperature to 800 °C of the freeze-dried CNT/NB hybrids: (A) p-MWCNT/NB and (B) P2-SWCNT/NB.

thus for a thermally reversible debundling and re-association of CNTs.

TGA (Fig. 3) further provided insights into the thermal degradation profiles of the hybrids. The results showed that the thermal degradation profiles of the hybrids closely resembled those of the NBs (Fig. S5C and D, ESI†), with similar onset degradation temperatures, but differing in terms of mass residue percentages at 800 °C. Since CNTs exhibit high thermal stability in a N_2 atmosphere, the observed degradation is primarily ascribed to the NBs present in the hybrids. CNT/ChNC hybrids present the lowest residue (33.9% for p-MWCNTs and 24.2% for P2-SWCNTs) likely due to a lower CNT concentration and an inherently higher degradability of ChNCs at 800 °C.[42] By contrast, CNT/CNC II dispersions exhibit the highest mass residues at 800 °C, followed by p-MWCNT/CNC I and P2-SWCNT/CNC I, highlighting the superior efficiency of type II CNCs over type I CNCs and ChNCs in stabilizing CNTs. Importantly, the TGA profiles of the hybrids after a thermal treatment (Fig. S6, ESI†) show negligible weight losses up to the range of 500–600 °C, thermally decomposing thereafter, which implies good thermal stability of the pyrolyzed hybrids.

Following these fundamental characterization studies, the CNT/NB dispersions, deemed hereafter as inks, were used to fabricate conductive films on glass substrates using spray coating, thus forming homogeneous layers (Fig. S7, ESI†). To remove the remaining non-conductive NBs while not harming the conductive CNT network, in agreement with TGA results, we carried out thermal treatment under a N_2 flow at 450 °C. An evaluation of the film thickness, R_S, and bulk conductivity (σ) before and after thermal treatment is shown in Table 2. Important differences were observed in σ among the

Table 2 Characterization values of films prepared by spray coating over glass substrates using the as-prepared CNT/NB inks before and after the thermal treatment. Eqn (S1) (ESI) was used to calculate σ values

		Before thermal treatment			After thermal treatment		
CNT	NBs	R_S (Ω $\square^{-1}$)	Thickness (μm)	σ (S cm^{-1})	R_S (Ω $\square^{-1}$)	Thickness (μm)	σ (S cm^{-1})
p-MWCNTs	ChNCs	79	4.3 ± 0.6	31	58	3.7 ± 0.2	46
	CNCs I	107	4.6 ± 0.5	20	64	2.2 ± 0.4	71
	CNCs II	73	2.7 ± 0.3	46	68	1.8 ± 0.2	82
P2-SWCNTs	ChNCs	130	4.0 ± 0.4	19	90	2.1 ± 03	28
	CNCs I	33	3.6 ± 0.3	108	20	2.8 ± 0.1	138
	CNCs II	18	5.3 ± 0.6	105	17	3.5 ± 0.1	168

different films, with p-MWCNT/ChNC films exhibiting higher σ (3.1 S cm^{-1}) than P2-SWCNT/ChNC films (0.4 S cm^{-1}). This difference is likely due to the heavier wrapping of the SWCNTs by ChNCs, as observed in TEM (Fig. 1A and B) and TGA (Fig. 3A and B). The combination of type I CNCs with p-MWCNTs results in somewhat more resistive films (20 S cm^{-1}). Moreover, P2-SWCNT/CNC I films display a notably higher σ (108 S cm^{-1}), possibly arising from the highly interconnected P2-SWCNT network structure as shown in the TEM image (Fig. 1D). Furthermore, a generally higher surface conductivity was obtained when using type II CNCs for the fabrication of CNT-based films. Finally, a thermal treatment of the films at 450 °C in a N_2 atmosphere led to a clear increase in electrical σ and a reduction in film thickness (Table 2) in all cases, which is believed to be caused by the pyrolysis of insulating NBs,[42] resulting in R_S values below 100 Ω $\square^{-1}$,[3,13,55] matching (and even surpassing) the performance of benchmark surface conductors at similar thicknesses, such as indium tin oxide (ITO, ~150–200 Ω $\square^{-1}$),[56] fluorinated tin oxide (FTO, ~100–200 Ω $\square^{-1}$),[57] aluminum-doped zinc oxide (AZO, ~100–200 Ω $\square^{-1}$),[58] or silver nanowires (AgNWs, ~2–40 Ω $\square^{-1}$).[59]

To assess the impact of the thermal treatment on the surface morphology of the films, SEM images were acquired before and after such post-treatment (Fig. 4). Prior to thermal treatment, CNTs were embedded within a NB matrix. After the thermal treatment (450 °C for 30 min under N_2), the CNTs became more exposed because of the removal of NBs,[42] which agrees with the observed reduction in film thickness and increased σ (Table 2). Furthermore, the homogeneity of the films is preserved after the thermal treatment, showing images with a high degree of compaction as well as uniform substrate coverage (Fig. S6, ESI†). These results, along with the fact that the films were produced by spray coating, a potential large-scale processing technique, underline the virtue of this method for developing conductive films with suitable electrical properties towards further application as carbon-based electrodes. This discussion is complemented with contact angle measurements (Fig. S8,ESI†), which hint at the changes in the surface chemistry of the films

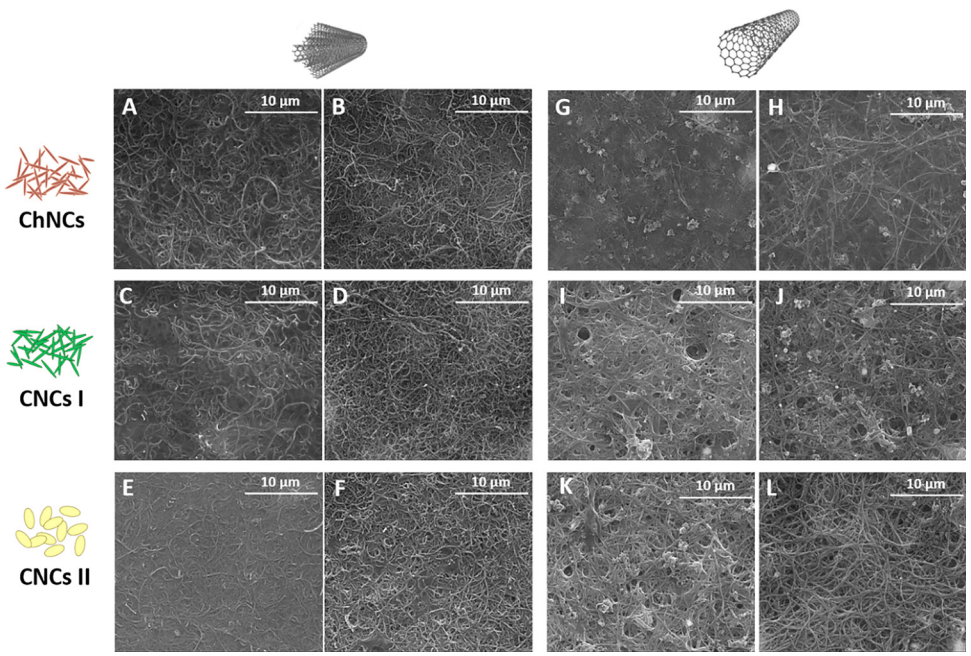

Fig. 4 SEM images of CNT/NB films: MWCNT-based films (A–F, left column) and SWCNT-based films (G–L, right column). Rows correspond to ChNCs (A, B and G, H, top), type I CNCs (C, D and I, J, middle), and type II CNC II (E, F and K, L, bottom). For each pair, untreated samples (A, C, E, G, J, K) are shown on the left and thermally treated ones (B, D, F, H, J, L) on the right.

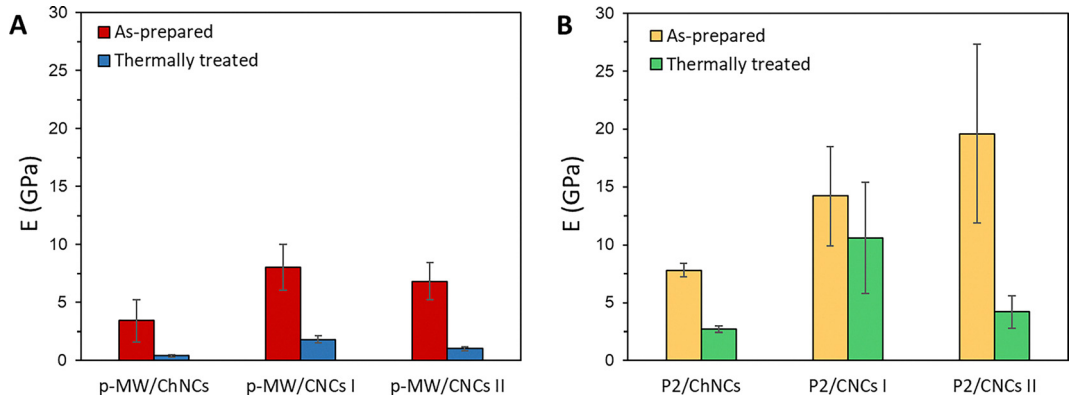

Fig. 5 Measured elastic moduli for (A) p-MWCNT/NB and (B) P2-SWCNT/NB.

upon thermal treatment through the wettability of their surfaces.

The results for mechanical characterization of the films are shown in Fig. 5 and in the ESI† (Fig. S9, S10 and Table S4). The as-produced P2-SWCNT/NB films present remarkably higher values of nanohardness and elastic moduli than their p-MWCNT/NB counterparts, regardless of the NB employed. Additionally, both mechanical parameters seem to be somehow affected by thermal treatment, leading to a diminution of mechanical performance. This diminution may be related to the partial removal of the NBs with the thermal treatment, leading to a more flexible structure. In partial opposition to this behavior, the treated P2-SWCNT/CNCs I films reflect an improvement in nanohardness (Fig. S9, ESI†) whilst diminish its elastic modulus value (Fig. 5).

At this point, the as-prepared films underwent electrochemical characterization to ensure their potential as functional electrodes for diverse applications. A straightforward technique for evaluating their electrochemical response is cyclic voltammetry (CV). Fig. 6 displays CVs of CNT/NB films before and after thermal treatment under an inert atmosphere, observing that the double layer capacitance increases in both MWCNT (Fig. 6a) and SWCNT (Fig. 6b) electrodes. These findings may hint at an increased accessible surface area of the electrodes, which was estimated through the calculation of the electrochemically active surface area (EASA). EASA is a useful parameter that can be employed in this case to assess the observed changes in the electrochemical activity of CNT/NB electrodes before and after thermal treatment. Such a parameter can be obtained from the double layer capacitance (C_{dl}) measured during CV measurements (see the ESI,† Fig. S11 and S12). Further details regarding the estimation of such a parameter are found in the ESI† (eqn (S2)–(S4) and Tables S5, S6).

The estimated EASA values given in $m^2\ g^{-1}$ are depicted in Fig. 7 for p-MWCNT/NB and P2-SWCNT/NB electrodes. In the case of p-MWCNT/NB electrodes (Fig. 7A), the EASA values increased upon thermal treatment. It should be noted that as-prepared p-MWCNT/NB electrodes display low EASA values due to the presence of insulating NBs within the film, which eventually results in an important blockage of their electrochemical active sites. Moreover, it seems that the thermal treatment influence is much more pronounced for P2-SWCNT/NB electrodes (Fig. 7B), resulting in films with larger EASA upon thermal treatment. Initially, P2-SWCNT/ChNC and P2-SWCNT/CNC I electrodes display a similar EASA as the morphology of both NBs is similar (*i.e.*, needle-shape

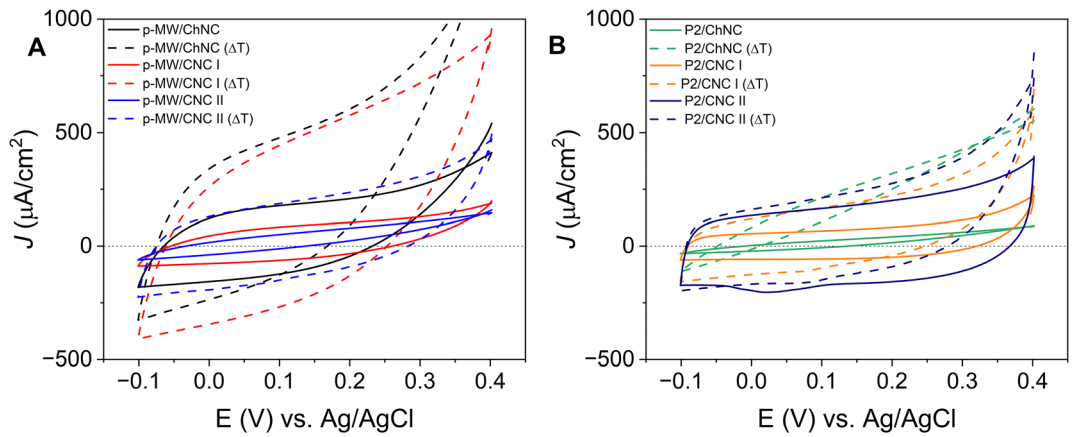

Fig. 6 Cyclic voltammetry measurements of (A) p-MWCNT/NB and (B) P2-SWCNT/NB electrodes at a scan rate of 50 mV s^{-1}. Note that solid lines correspond to the as-prepared electrodes, whereas dashed lines represent thermally treated samples.

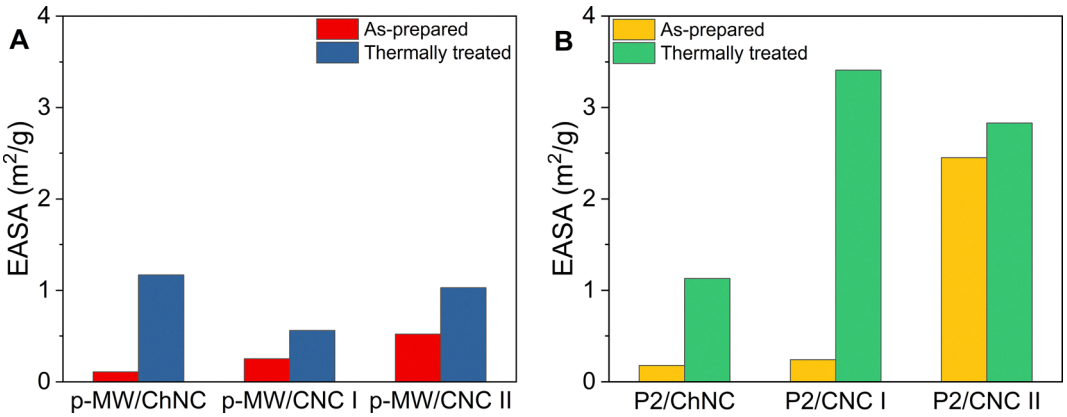

Fig. 7 Estimated EASA for (A) p-MWCNT/NB and (B) P2-SWCNT/NB electrodes.

morphology). The case of P2-SWCNT/CNC II electrodes is notably different due to the particular morphology of CNC II (*i.e.*, rod-like shape). This leads to a totally different interaction with P2-SWCNT, resulting in electrodes that show that the remarkable EASAs as type II CNCs are seemingly not blocking the active sites of P2-SWCNTs as much as the rest of cases.

From these results, it can be inferred that the thermal treatment effect in P2-SWCNT electrodes is more pronounced when using type I CNCs and type II CNCs, thus agreeing with the TGA observations (Fig. 3B). This fact results in an effective pyrolysis of both CNC types that eventually facilitates the entrance of the electrolyte into the film pores, thereby showing larger EASA values. The observed variability of the electrochemical response in p-MWCNT/NB and P2-SWCNT/NB electrodes highlight the importance of considering both the electrical conductivities and the EASAs when designing high-performance electrodes. In fact, these differences underscore the intricate relationships between the structural configuration of CNTs and NBs, and their subsequent impact on the electrolyte accessibility, which can affect the overall performance of the electrodes.

Aiming to further evaluate the electrochemical properties of the as-prepared films, electrochemical impedance spectroscopy measurements were carried out (Fig. S13, ESI†). From the Nyquist plot, two main contributions can be observed: series resistance and electrolytic diffusion. While the former is mostly related to the electrical conductivity of the electrode, the latter is mainly ruled by their EASA. In this sense, thermally treated electrodes tend to display lower values of series resistance due to the absence of NBs within the film, which agrees with the electrical conductivity improvement after thermal treatment (Table 2) as well as with the morphology evidenced in SEM images (Fig. 4). Diffusion phenomena, moreover, is strongly dependent on the combination of both the CNT and the NB employed. As a general trend, it seems that the electrolytic diffusion at the electrode/electrolyte interface is more favored when NBs have been previously pyrolyzed. This fact can be ascertained according to the slope position of the impedance, being also slightly tilted in the case of thermally treated electrodes. These observations are in line with the estimation of the EASA as shown in Fig. 7, in which thermally treated electrodes reveal larger EASAs and thus enhanced diffusion at the electrode/electrolyte interface.

Conclusions

The present work successfully showcased a general approach for fabricating functional CNT film electrodes by using NBs as effective dispersants in aqueous media. Through the use of ChNCs or CNCs, stable waterborne inks of either SWCNTs or MWCNTs are obtained and then processed into conductive films. An appropriate choice of the NB during the ink preparation and subsequent thermal treatment of the film is of special interest, as it significantly impacts the resulting structural, electrical, and electrochemical properties of the electrodes thereof. Specifically, type II CNCs exhibited superior performance in stabilizing CNTs, leading to films with higher electrical conductivity. A conceptual application of these aqueous inks allows the fabrication of film electrodes by ink deposition on glass substrates through spray coating. We further demonstrate that the thermal treatment of the applied films at 450 °C in a N_2 atmosphere pyrolyzes the non-conductive NB while leaving exposed the CNT networks, resulting in more conductive electrodes, provided with different electrochemical features. Through cyclic voltammetry experiments, we estimated the electrochemically active surface area, a relevant parameter that indicates the capabilities of these film electrodes for further applications. In this sense, we clearly observed that the structural, morphological and electrical properties of the CNT/NB hybrids significantly affect the electrochemical behavior of the resulting film electrodes. These findings unveil the potential of the proposed strategy for developing carbon-based conductive and electroactive nanohybrids processed entirely in aqueous media. The as-prepared film electrodes are suitable for potential device components in a variety of applications, playing roles such as electrochemically active units in energy generation or storage systems, as well as current collectors in electrochemical and photoelectrochemical devices.

Conflicts of interest

There are no conflicts of interest to declare.

Data availability

The data supporting this article have been included as part of the ESI.†

Acknowledgements

Financial support from the Spanish MCIN/AEI/10.13039/501100011033 and ''ERDF A way of making Europe'' by the European Union under project grants PID2022-139671OB-I00 and PID2023-147116OB-I00, as well as from the Gobierno de Aragón (DGA), in the R&D&I projects in priority lines and of a multidisciplinary nature (project grant PROY_T41_24), and through the grants to research groups (Grupo Reconocido DGA-T03_23R) is acknowledged. C. M.-B., V. C. and M. Á. Á.-S. thank the DGA for funding their PhD contracts (refs. CUS/621/2023, CUS/581/2020 and IIU/796/2019, respectively).

References

1 V. Schroeder, S. Savagatrup, M. He, S. Lin and T. M. Swager, Carbon Nanotube Chemical Sensors, *Chem. Rev.*, 2019, **119**(1), 599–663, DOI: **10.1021/acs.chemrev.8b00340**.

2 S. Lu, B. N. Smith, H. Meikle, M. J. Therien and A. D. Franklin, All-Carbon Thin-Film Transistors Using Water-Only Printing, *Nano Lett.*, 2023, **23**(6), 2100–2106, DOI: **10.1021/acs.nanolett.2c04196**.

3 A. Ansón-Casaos, O. Sanahuja-Parejo, J. Hernández-Ferrer, A. M. Benito and W. K. Maser, Carbon Nanotube Film Electrodes with Acrylic Additives: Blocking Electrochemical Charge Transfer Reactions, *Nanomaterials*, 2020, **10**(6), 1078, DOI: **10.3390/nano10061078**.

4 I. Jeon, T. Chiba, C. Delacou, Y. Guo, A. Kaskela, O. Reynaud, E. I. Kauppinen, S. Maruyama and Y. Matsuo, Single-Walled Carbon Nanotube Film as Electrode in Indium-Free Planar Heterojunction Perovskite Solar Cells: Investigation of Electron-Blocking Layers and Dopants, *Nano Lett.*, 2015, **15**(10), 6665–6671, DOI: **10.1021/acs.nanolett.5b02490**.

5 E. Contreras, D. Dominguez, H. Tiznado, J. Guerrero-Sanchez, N. Takeuchi, G. Alonso-Nunez, O. E. Contreras, M. T. Oropeza-Guzmán and J. M. Romo-Herrera, N-Doped Carbon Nanotubes Enriched with Graphitic Nitrogen in a Buckypaper Configuration as Efficient 3D Electrodes for Oxygen Reduction to H_2O_2, *Nanoscale*, 2019, **11**(6), 2829–2839, DOI: **10.1039/c8nr08384c**.

6 N. Shahzad, Z. Lutfullah, T. Perveen, D. Pugliese, S. Haq, N. Fatima, S. M. Salman, A. Tagliaferro and M. I. Shahzad, Counter Electrode Materials Based on Carbon Nanotubes for Dye-Sensitized Solar Cells, *Renewable Sustainable Energy Rev.*, 2022, 112196, DOI: **10.1016/j.rser.2022.112196**.

7 D. Jović, V. Jaćević, K. Kuča, I. Borišev, J. Mrdjanovic, D. Petrovic, M. Seke and A. Djordjevic, The Puzzling Potential of Carbon Nanomaterials: General Properties, Application, and Toxicity, *Nanomaterials*, 2020, **10**(8), 1508, DOI: **10.3390/nano10081508**.

8 V. Meunier, A. G. Souza Filho, E. B. Barros and M. S. Dresselhaus, Physical Properties of Low-Dimensional Sp2 -Based Carbon Nanostructures, *Rev. Mod. Phys.*, 2016, **88**(2), 025005, DOI: **10.1103/RevModPhys.88.025005**.

9 A. Ansón-Casaos, R. Mis-Fernández, C. M. López-Alled, E. Almendro-López, J. Hernández-Ferrer, J. M. González-Domínguez and M. T. Martínez, Transparent Conducting Films Made of Different Carbon Nanotubes, Processed Carbon Nanotubes, and Graphene Nanoribbons, *Chem. Eng. Sci.*, 2015, **138**, 566–574, DOI: **10.1016/j.ces.2015.09.002**.

10 L. Hu, D. S. Hecht and G. Grüner, Carbon Nanotube Thin Films: Fabrication, Properties, and Applications, *Chem. Rev.*, 2010, **110**(10), 5790–5844, DOI: **10.1021/cr9002962**.

11 O. Kanoun, C. Müller, A. Benchirouf, A. Sanli, T. N. Dinh, A. Al-Hamry, L. Bu, C. Gerlach and A. Bouhamed, Flexible Carbon Nanotube Films for High Performance Strain Sensors, *Sensors*, 2014, **14**(6), 10042–10071, DOI: **10.3390/s140610042**.

12 I. Jeon, T. Chiba, C. Delacou, Y. Guo, A. Kaskela, O. Reynaud, E. I. Kauppinen, S. Maruyama and Y. Matsuo, Single-Walled Carbon Nanotube Film as Electrode in Indium-Free Planar Heterojunction Perovskite Solar Cells: Investigation of Electron-Blocking Layers and Dopants, *Nano Lett.*, 2015, **15**(10), 6665–6671, DOI: **10.1021/acs.nanolett.5b02490**.

13 Y. Liao, R. Zhang, H. Wang, S. Ye, Y. Zhou, T. Ma, J. Zhu, L. D. Pfefferle and J. Qian, Highly Conductive Carbon-Based Aqueous Inks toward Electroluminescent Devices, Printed Capacitive Sensors and Flexible Wearable Electronics, *RSC Adv.*, 2019, **9**(27), 15184–15189, DOI: **10.1039/c9ra01721f**.

14 C. Pramanik, J. R. Gissinger, S. Kumar and H. Heinz, Carbon Nanotube Dispersion in Solvents and Polymer Solutions: Mechanisms, Assembly, and Preferences, *ACS Nano*, 2017, **11**(12), 12805–12816, DOI: **10.1021/acsnano.7b07684**.

15 L. Pokrajac, A. Abbas, W. Chrzanowski, G. M. Dias, B. J. Eggleton, S. Maguire, E. Maine, T. Malloy, J. Nathwani, L. Nazar, A. Sips, J. Sone, A. van den Berg, P. S. Weiss and S. Mitra, Nanotechnology for a Sustainable Future: Addressing Global Challenges with the International Network4Sustainable Nanotechnology, *ACS Nano*, 2021, **15**(12), 18608–18623, DOI: **10.1021/acsnano.1c10919**.

16 H. Jung, S. Y. An, J. S. Lim and D. Kim, Transparent Conductive Thin Film Synthesis Based on Single-Walled Carbon Nanotubes Dispersion Containing Polymethylmethacrylate Binder, *J. Nanosci. Nanotechnol.*, 2011, **11**, 6345–6349, DOI: **10.1166/jnn.2011.4439**.

17 D. Y. Cho, K. Eun, S. H. Choa and H. K. Kim, Highly Flexible and Stretchable Carbon Nanotube Network Electrodes Prepared by Simple Brush Painting for Cost-Effective Flexible Organic Solar Cells, *Carbon*, 2014, **66**, 530–538, DOI: **10.1016/j.carbon.2013.09.035**.

18 Q. Jin, B. Ren, H. Cui and C. Wang, Nitrogen and Cobalt Co-Doped Carbon Nanotube Films as Binder-Free Trifunctional Electrode for Flexible Zinc-Air Battery and Self-Powered Overall Water Splitting, *Appl. Catal., B*, 2021, **283**, 119643, DOI: 10.1016/j.apcatb.2020.119643.
19 V. Calvo, C. Martínez-Barón, L. Fuentes, W. K. Maser, A. M. Benito and J. M. González-Domínguez, Nanocellulose: The Ultimate Green Aqueous Dispersant for Nanomaterials, *Polymers*, 2024, **16**(12), 1664, DOI: 10.3390/polym16121664.
20 J. Jacob, J. T. Haponiuk, S. Thomas and S. Gopi, Biopolymer Based Nanomaterials in Drug Delivery Systems: A Review, *Mater. Today Chem.*, 2018, **9**, 43–55, DOI: 10.1016/j.mtchem.2018.05.002.
21 T. Jin, T. Liu, E. Lam and A. Moores, Chitin and Chitosan on the Nanoscale, *Nanoscale Horiz.*, 2021, **6**(7), 505–542, DOI: 10.1039/d0nh00696c.
22 D. Klemm, F. Kramer, S. Moritz, T. Lindström, M. Ankerfors, D. Gray and A. Dorris, Nanocelluloses: A New Family of Nature-Based Materials, *Angew. Chem., Int. Ed.*, 2011, **50**(24), 5438–5466, DOI: 10.1002/anie.201001273.
23 M. Nasrollahzadeh, M. Sajjadi, S. Iravani and R. S. Varma, Starch, Cellulose, Pectin, Gum, Alginate, Chitin and Chitosan Derived (Nano)Materials for Sustainable Water Treatment: A Review, *Carbohydr. Polym.*, 2021, **251**, 116986, DOI: 10.1016/j.carbpol.2020.116986.
24 B. Thomas, M. C. Raj, A. K. B, R. M. H, J. Joy, A. Moores, G. L. Drisko and C. Sanchez, Nanocellulose, a Versatile Green Platform: From Biosources to Materials and Their Applications, *Chem. Rev.*, 2018, **118**(24), 11575–11625, DOI: 10.1021/acs.chemrev.7b00627.
25 H. Marta, D. I. Rizki, E. Mardawati, M. Djali, M. Mohammad and Y. Cahyana, Starch Nanoparticles: Preparation, Properties and Applications, *Polymers*, 2023, **15**(5), 1167, DOI: 10.3390/polym15051167.
26 Q. Wang, S. Yan, G. Han, X. Li, R. You, Q. Zhang, M. Li and D. L. Kaplan, Facile Production of Natural Silk Nanofibers for Electronic Device Applications, *Compos. Sci. Technol.*, 2020, **187**, 107950, DOI: 10.1016/j.compscitech.2019.107950.
27 S. Mohammadzadehmoghadam and Y. Dong, Electrospinning of Silk Fibroin-Based Nanofibers and Their Applications in Tissue Engineering, in *Electrospun Polymers and Composites*, ed. Dong, Y., Baji, A., Ramakrishna, S., Elsevier, 2021, pp. 111–146, DOI: 10.1016/B978-0-12-819611-3.00004-2.
28 Y. Hu, Y. Zou, Y. Ma, J. Yu, L. Liu, M. Chen, S. Ling and Y. Fan, Formulation of Silk Fibroin Nanobrush-Stabilized Biocompatible Pickering Emulsions, *Langmuir*, 2022, **38**(46), 14302–14312, DOI: 10.1021/acs.langmuir.2c02376.
29 M. Kang, P. Chen and H.-J. Jin, Preparation of Multiwalled Carbon Nanotubes Incorporated Silk Fibroin Nanofibers by Electrospinning, *Curr. Appl. Phys.*, 2009, **9**(1), S95–S97, DOI: 10.1016/j.cap.2008.08.014.
30 N. C. Seeman, Nanomaterials Based on DNA, *Annu. Rev. Biochem.*, 2010, **79**(1), 65–87, DOI: 10.1146/annurev-biochem-060308-102244.
31 W. Ma, Y. Zhan, Y. Zhang, C. Mao, X. Xie and Y. Lin, The Biological Applications of DNA Nanomaterials: Current Challenges and Future Directions, *Signal Transduction Targeted Ther.*, 2021, **6**(1), 351, DOI: 10.1038/s41392-021-00727-9.
32 C. Olivier, C. Moreau, H. Bizot, B. Cathala and O. Chauvet, Cellulose Nanocrystals Mediated Dispersion of Single Walled Carbon Nanotubes (SWNTs) and Elaboration of SWNTs/Cellulose Nanocrystals Multilayered Thin Films, *MRS Proc.*, 2011, **1362**, 13–18, DOI: 10.1557/opl.2011.885.
33 C. Olivier, C. Moreau, P. Bertoncini, H. Bizot, O. Chauvet and B. Cathala, Cellulose Nanocrystal-Assisted Dispersion of Luminescent Single-Walled Carbon Nanotubes for Layer-by-Layer Assembled Hybrid Thin Films, *Langmuir*, 2012, **28**(34), 12463–12471, DOI: 10.1021/la302077a.
34 J. M. González-Domínguez, A. Ansón-Casaos, L. Grasa, L. Abenia, A. Salvador, E. Colom, J. E. Mesonero, J. E. García-Bordejé, A. M. Benito and W. K. Maser, Unique Properties and Behavior of Nonmercerized Type-II Cellulose Nanocrystals as Carbon Nanotube Biocompatible Dispersants, *Biomacromolecules*, 2019, **20**(8), 3147–3160, DOI: 10.1021/acs.biomac.9b00722.
35 V. Calvo, A. J. Paleo, J. M. González-Domínguez, E. Muñoz, B. Krause, P. Pötschke, W. K. Maser and A. M. Benito, The Aqueous Processing of Carbon Nanofibers via Cellulose Nanocrystals as a Green Path towards E-Textiles with n-Type Thermoelectric Behaviour, *Carbon*, 2024, **217**, 118640, DOI: 10.1016/j.carbon.2023.118640.
36 J. B. Mougel, C. Adda, P. Bertoncini, I. Capron, B. Cathala and O. Chauvet, Highly Efficient and Predictable Noncovalent Dispersion of Single-Walled and Multi-Walled Carbon Nanotubes by Cellulose Nanocrystals, *J. Phys. Chem. C*, 2016, **120**(39), 22694–22701, DOI: 10.1021/acs.jpcc.6b07289.
37 V. Calvo, M. Á. Álvarez Sánchez, L. Güemes, C. Martínez-Barón, S. Baúlde, A. Criado, J. M. González-Domínguez, W. K. Maser and A. M. Benito, Preparation of Cellulose Nanocrystals: Controlling the Crystalline Type by One-Pot Acid Hydrolysis, *ACS Macro Lett.*, 2023, **12**(2), 152–158, DOI: 10.1021/acsmacrolett.2c00705.
38 S. Dortez, T. Sierra, M. Á. Álvarez-Sánchez, J. M. González-Domínguez, A. M. Benito, W. K. Maser, A. G. Crevillen and A. Escarpa, Effect of Nanocellulose Polymorphism on Electrochemical Analytical Performance in Hybrid Nanocomposites with Non-Oxidized Single-Walled Carbon Nanotubes, *Microchim. Acta*, 2022, **189**(2), 62, DOI: 10.1007/s00604-021-05161-w.
39 C. Olivier, J. B. Mougel, P. Bertoncini, C. Moreau, I. Capron, B. Cathala and O. Chauvet, Carbon Nanotube/Cellulose Nanocrystal Hybrid Conducting Thin Films, *J. Renew. Mater.*, 2017, **6**(3), 237–241, DOI: 10.7569/JRM.2017.634168.
40 J. M. González-Domínguez, L. Grasa, J. Frontiñán-Rubio, E. Abás, A. Domínguez-Alfaro, J. E. Mesonero, A. Criado and A. Ansón-Casaos, Intrinsic and Selective Activity of Functionalized Carbon Nanotube/Nanocellulose Platforms against Colon Cancer Cells, *Colloids Surf., B*, 2022, **212**, 112363, DOI: 10.1016/j.colsurfb.2022.112363.
41 Y. He, X. Lin, Y. Feng, B. Luo and M. Liu, Carbon Nanotube Ink Dispersed by Chitin Nanocrystals for Thermoelectric Converter for Self-Powering Multifunctional Wearable

Electronics, *Adv. Sci.*, 2022, **9**(33), 2204675, DOI: **10.1002/advs.202204675**.

42 V. Calvo, C. Martínez-Barón, B. Vázquez-Conejo, A. Dominguez-Alfaro, A. J. Paleo, B. Villacampa, A. Ansón-Casaos, W. K. Maser, A. M. Benito and J. M. González-Domínguez, Carbon Nanomaterials-Based Inks and Electrodes Using Chitin Nanocrystals, *ACS Sustain. Chem. Eng.*, 2024, **12**(43), 15980–15990, DOI: **10.1021/acssuschemeng.4c05253**.

43 H. Koga, T. Saito, T. Kitaoka, M. Nogi, K. Suganuma and A. Isogai, Transparent, Conductive, and Printable Composites Consisting of TEMPO-Oxidized Nanocellulose and Carbon Nanotube, *Biomacromolecules*, 2013, **14**(4), 1160–1165, DOI: **10.1021/bm400075f**.

44 M. M. Hamedi, A. Hajian, A. B. Fall, K. Håkansson, M. Salajkova, F. Lundell, L. Wågberg and L. A. Berglund, Highly Conducting, Strong Nanocomposites Based on Nanocellulose-Assisted Aqueous Dispersions of Single-Wall Carbon Nanotubes, *ACS Nano*, 2014, **8**(3), 2467–2476, DOI: **10.1021/nn4060368**.

45 A. Hajian, S. B. Lindström, T. Pettersson, M. M. Hamedi and L. Wågberg, Understanding the Dispersive Action of Nanocellulose for Carbon Nanomaterials, *Nano Lett.*, 2017, **17**(3), 1439–1447, DOI: **10.1021/acs.nanolett.6b04405**.

46 Y. Li, H. Zhu, Y. Wang, U. Ray, S. Zhu, J. Dai, C. Chen, K. Fu, S. Jang, D. Henderson, T. Li and L. Hu, Cellulose-Nanofiber-Enabled 3D Printing of a Carbon-Nanotube Microfiber Network, *Small Methods*, 2017, **1**(10), 1700222, DOI: **10.1002/smtd.201700222**.

47 V. Kuzmenko, E. Karabulut, E. Pernevik, P. Enoksson and P. Gatenholm, Tailor-Made Conductive Inks from Cellulose Nanofibrils for 3D Printing of Neural Guidelines, *Carbohydr. Polym.*, 2018, **189**, 22–30, DOI: **10.1016/j.carbpol.2018.01.097**.

48 H. Zhang, X. Sun, Z. Heng, Y. Chen, H. Zou and M. Liang, Robust and Flexible Cellulose Nanofiber/Multiwalled Carbon Nanotube Film for High-Performance Electromagnetic Interference Shielding, *Ind. Eng. Chem. Res.*, 2018, **57**(50), 17152–17160, DOI: **10.1021/acs.iecr.8b04573**.

49 C. Pan, Q. Xie, Z. Hu, M. Yang and L. Zhu, Mechanical and Biological Properties of Silk Fibroin/Carbon Nanotube Nanocomposite Films, *Fibers Polym.*, 2015, **16**(8), 1781–1787, DOI: **10.1007/s12221-015-5185-1**.

50 H.-S. Kim, S. H. Yoon, S.-M. Kwon and H.-J. Jin, PH-Sensitive Multiwalled Carbon Nanotube Dispersion with Silk Fibroins, *Biomacromolecules*, 2009, **10**(1), 82–86, DOI: **10.1021/bm800896e**.

51 M. T. Martínez, M. A. Callejas, A. M. Benito, M. Cochet, T. Seeger, A. Ansón, J. Schreiber, C. Gordon, C. Marhic, O. Chauvet, J. L. G. Fierro and W. K. Maser, Sensitivity of Single Wall Carbon Nanotubes to Oxidative Processing: Structural Modification, Intercalation and Functionalisation, *Carbon*, 2003, **41**(12), 2247–2256, DOI: **10.1016/S0008-6223(03)00250-1**.

52 J. M. González-Domínguez, P. Castell, A. Ansón, W. K. Maser, A. M. Benito and M. T. Martinez, Block Copolymer Assisted Dispersion of Single Walled Carbon Nanotubes and Integration into a Trifunctional Epoxy, *J. Nanosci. Nanotechnol.*, 2009, **9**(10), 6104–6112, DOI: **10.1166/jnn.2009.1575**.

53 A. Santidrián, M. Kierkowicz, E. Pach, D. Darvasiová, B. Ballesteros, G. Tobias and M. Kalbáč, Charge Transfer in Steam Purified Arc Discharge Single Walled Carbon Nanotubes Filled with Lutetium Halides, *Phys. Chem. Chem. Phys.*, 2020, **22**(18), 10063–10075, DOI: **10.1039/D0CP01408G**.

54 Y. Maniwa, R. Fujiwara, H. Kira, H. Tou, H. Kataura, S. Suzuki, Y. Achiba, E. Nishibori, M. Takata, M. Sakata, A. Fujiwara and H. Suematsu, Thermal Expansion of Single-Walled Carbon Nanotube (SWNT) Bundles: X-Ray Diffraction Studies, *Phys. Rev. B:Condens. Matter Mater. Phys.*, 2001, **64**(24), 241402, DOI: **10.1103/PhysRevB.64.241402**.

55 J. M. González-Domínguez, A. Baigorri, M. Á. Álvarez-Sánchez, E. Colom, B. Villacampa, A. Ansón-Casaos, E. García-Bordejé, A. M. Benito and W. K. Maser, Waterborne Graphene- and Nanocellulose-Based Inks for Functional Conductive Films and 3D Structures, *Nanomaterials*, 2021, **11**(6), 1435, DOI: **10.3390/nano11061435**.

56 D.-P. Tran, H.-I. Lu and C.-K. Lin, Conductive Characteristics of Indium Tin Oxide Thin Film on Polymeric Substrate under Long-Term Static Deformation, *Coatings*, 2018, **8**(6), 212, DOI: **10.3390/coatings8060212**.

57 J. Q. Tian; H. Y. Shi and W. Zheng, Synthesis and Characterization of Fluorine-Doped Tin Oxide Nanocrystals Prepared by Sol-Gel Method, *Advanced Materials Research*, Trans Tech Publications Ltd, 2014, vol. 977, pp. 59–62, DOI: **10.4028/www.scientific.net/AMR.977.59**.

58 Z. Zhu, T. Mankowski, K. Balakrishnan, A. S. Shikoh, F. Touati, M. A. Benammar, M. Mansuripur and C. M. Falco, Sol-Gel Deposited Aluminum-Doped and Gallium-Doped Zinc Oxide Thin-Film Transparent Conductive Electrodes with a Protective Coating of Reduced Graphene Oxide, *J. Nanophotonics*, 2016, **10**(2), 026001, DOI: **10.1117/1.JNP.10.026001**.

59 D. Kumar, V. Stoichkov, E. Brousseau, G. C. Smith and J. Kettle, High Performing AgNW Transparent Conducting Electrodes with a Sheet Resistance of 2.5 Ω Sq^{-1} Based upon a Roll-to-Roll Compatible Post-Processing Technique, *Nanoscale*, 2019, **11**(12), 5760–5769, DOI: **10.1039/C8NR07974A**.